Highly Dispersive Scattering from Defects in Noncollinear Magnets

Wolfram Brenig and A. L. Chernyshev

Phys. Rev. Lett. **110**, 157203 — Published 9 April 2013

DOI: 10.1103/PhysRevLett.110.157203

Highly Dispersive Scattering From Defects In Non-Collinear Magnets

Wolfram Brenig[1,*] and A. L. Chernyshev[2]

[1] *Institut für Theoretische Physik, Technische Universität Braunschweig, 38106 Braunschweig, Germany*
[2] *Department of Physics, University of California, Irvine, California 92697, USA*

We demonstrate that point-like defects in non-collinear magnets give rise to a highly dispersive structure in the magnon scattering, violating a standard paradigm of its momentum independence. For a single impurity spin coupled to a prototypical non-collinear antiferromagnet, we find that the resolvent is dominated by a distinct dispersive structure with its momentum-dependence set by the magnon dispersion and shifted by the ordering vector. This feature is a consequence of umklapp scattering off the impurity-induced *spin texture*, which arises due to the non-collinear ground state of the host system. Detailed results for the staggered and uniform magnetization of this texture as well as the T-matrix from numerical linear spin-wave theory are presented.

PACS numbers: 75.10.Jm, 75.40.Gb, 78.70.Nx, 75.50.Ee

Introduction.—Electron localization [1], paramagnetic impurities in superconductors [2], and the orthogonality catastrophe [3], all attest to the fundamental importance of impurities as probes of quantum many-body systems. Major research effort in cuprate superconductors has led to extensive studies of impurities in the square-lattice Heisenberg antiferromagnets (HAFs), uncovering new universality classes for disorder-driven transitions [4–8], impurity-induced magnetic order [9], fractional Curie response [10, 11], and anomalous low-energy magnon scattering [12, 13].

While the square-lattice HAF is unfrustrated and has a collinear ground state, defects in non-collinear and frustrated quantum magnets have come into focus only recently, displaying an even richer physics. This includes frustration release, dimer freezing, and mutual impurity repulsion [14–16], valence bond glass states [17, 18], emergent gauge-flux pinning [19], breakdown of linear response [20], fractional impurity moments, and — the primary topic of this Letter — spin textures [21–23].

Impurity-induced spin textures are a genuine hallmark of non-collinear magnetic order and can be understood on a purely classical level. Removing a spin from the host, or adding an extra defect spin, locally perturbs the balance of exchange fields and requires the surrounding spins of the non-collinear host to readjust their directions recursively, resulting in a long-ranged modification of the canting angles, i.e., a texture [21–23]. A 1D sketch of this is shown in Figs. 1(b) and (c) for the field-induced non-collinear state coupled to an impurity spin. The readjustment effect is absent for collinear order, where impurity spin simply co-aligns with the host, as in Fig. 1(a). In contrast to that, the texture implies a fractional screening of the impurity moment [22]. The real-space decay of the texture depends on the nature of the non-collinear state. In a field-induced canted states, textures decay exponentially on a length scale inversely proportional to the external field [21]. In frustration-induced non-collinear states, Goldstone modes lead to an algebraic decay of the texture [22–24].

In this Letter we advance the field beyond previous studies, which have focused on the static properties of defects, and investigate magnon impurity-scattering in non-collinear magnets. To be specific, we consider the field-induced canted state of the square-lattice HAF with an additional defect, namely an extra out-of-plane spin interacting by an exchange coupling with one of the host spins. We discover a phenomenon rather surprising, if confronted with conventional expectations for the scattering amplitude from a point defect, which is either momentum-independent altogether, aside from the trivial transformation of the excitation basis, or contains only a broad momentum modulation due superposition of a few partial waves. Instead, the scattering amplitude displays a strongly dispersive feature, clearly tracing the magnon dispersion shifted by the magnetic ordering vec-

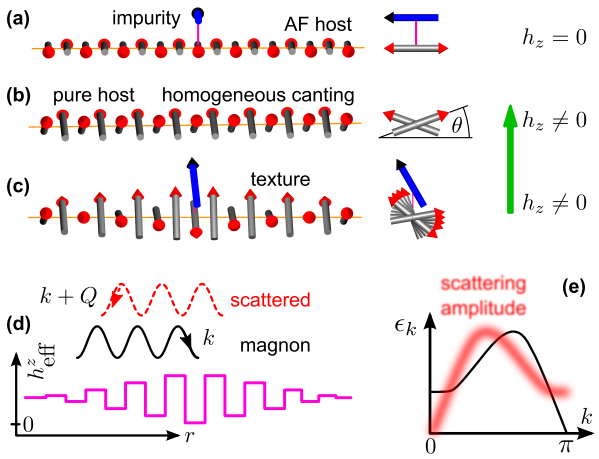

FIG. 1. (color online) (a) Impurity spin coupled to a collinear state: all spins co-aligned. (b) Homogeneous canted state in external field h_z. (c) Impurity spin coupled to the canted state: host spins readjust, creating a texture. (d) 1D sketch of umklapp scattering by the texture, which generates staggered z-component of the effective field with the wave vector $Q = \pi$. (e) Solid black line: magnon dispersion; blurred red line: dispersive peak in scattering amplitude.

tor. We show that this effect is an unequivocal consequence of the spin texture. Intuitively, an effective staggering of the magnetic field is generated by the texture, made explicit in Fig. 1(d). This serves as a potential for umklapp scattering of magnons, which, in turn, leads to the central new feature in the T-matrix — a momentum-dependent resonance. In the following, we provide the detailed arguments for this result, which should remain valid for a wide class of frustrated non-collinear systems, and suggest experiments to test this prediction.

Model.—We consider the square-lattice HAF at $T=0$ in an external field, coupled to an impurity spin $\mathbf{S}'$

$$\mathcal{H} = J_0 \sum_{\langle lm \rangle} \mathbf{S}_l \cdot \mathbf{S}_m - h \sum_l S_l^z + J \mathbf{S}_0 \cdot \mathbf{S}_i' - h\, S_i'^z \,, \quad (1)$$

where $\langle lm \rangle$ are the nearest-neighbor bonds of the square lattice, the exchange couplings of the host (J_0) and host-to-impurity (J) are antiferromagnetic. The gyromagnetic ratio is identical for all spins and is included into the magnetic field h. In the following, we set $J_0 = 1$.

The spin configuration that minimizes the classical energy of model (1) at $h\neq 0$ corresponds to an inhomogeneous distribution of spin tilt angles θ_l out of the xy-plane where ordering occurs at $h=0$, see Fig. 1. For a $1/S$ expansion, we align the local spin quantization axis on each site in the direction given by the local canted frame [25, 26]. The rotation of spin components from the laboratory frame (x_0, y_0, z_0) is given by $S_l^{y_0} = S_l^y$ and $S_l^{x_0(z_0)} = S_l^{x(z)} \sin\theta_l \pm S_l^{z(x)} e^{i\mathbf{Q}\cdot\mathbf{r}_l} \cos\theta_l$, where $\mathbf{Q} = (\pi, \pi)$ is the Néel ordering wave-vector. The transformation is the same for the impurity spin $\mathbf{S}_i'$ as it can be seen as a neighbor of the site $l=0$, which it is coupled to.

Expressing the spin operators in terms of Holstein-Primakoff bosons, Hamiltonian (1) is transformed into a series $\mathcal{H} = \mathcal{H}_{\rm class} + \mathcal{H}_1 + \mathcal{H}_2 + ...$ with decreasing powers of $S(S')$ and increasing number of boson operators. Each term in this series depends on all $\theta_{\{l\}}$ and $\mathcal{H}_{\rm class}$ is the classical energy [27]. The harmonic spin-wave term is $\mathcal{H}_2$ and stability requires $\mathcal{H}_1 \equiv 0$. Equivalently, the ground state must minimize $\mathcal{H}_{\rm class}$, i.e. $\partial\mathcal{H}_{\rm class}/\partial\theta_{\{l\}} = 0$. Without the impurity, all $\theta_l \equiv \sin^{-1}(h/h_s)$ with the saturation field $h_s = 8S$ [25]. With the impurity, minimization gives a set of nonlinear coupled equations, which determine the inhomogeneous distribution of the local tilt angles θ_l — referred to as the *texture* hereafter.

In what follows, we study the properties of this texture numerically in finite $N \times N$ clusters with periodic boundary conditions. First, we briefly address its static properties and then turn to its quantum dynamics using numerical real-space diagonalization of $\mathcal{H}_2$.

Classical texture.—Here we characterize the *classical* ground state, which is sufficient for our subsequent evaluation of the quantum dynamics [20–22]. The spatial extent and field-dependence of the texture can be described in terms of the *staggered* z-component of the magnetization $m^z_{stag,\mathbf{r}_l}$ obtained from the set of $\sin(\theta_l)$. Our results, inset (b) of Fig. 2 and [27], largely corroborate earlier findings of [21], where $m^z_{stag,\mathbf{r}_l}$ was investigated by a continuum theory and quantum Monte Carlo for a different impurity type. In particular, the texture decays exponentially at $|\mathbf{r}_l| \gg 1$, consistent with the impurity not coupled to the Goldstone mode of the host system.

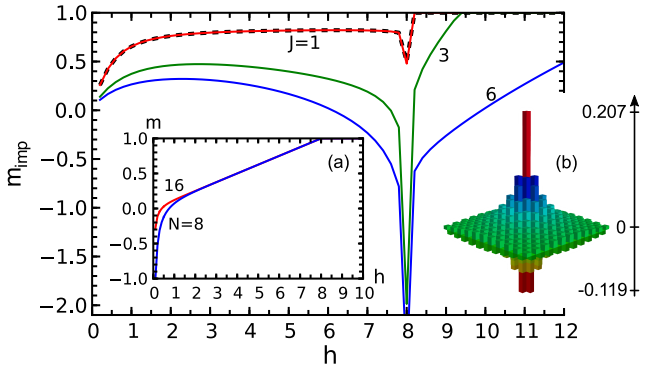

FIG. 2. (color online) Impurity magnetization m_{imp} vs h for J=1, 3, and 6 in N=72 cluster and for J=1 in N=64 cluster (dashed). Insets: (a) Local magnetization m_l^z at the distance $(N/2, N/2)$ from $l=0$ in $N=8$ and 16 clusters for J=1. (b) Local magnetization $\Delta m_l^z = (\sin(\theta_0) - \sin(\theta_l))$ in a 21×21 section of the N=72 cluster, for J=1, h=0.4.

Fig. 2 shows another characteristics of the texture: the impurity contribution to the *uniform* magnetization $m_{imp} = m^z - m^z_{host}$ vs field for several values of the coupling J. Here $m^z = \sum_n S_n^z$ is the uniform magnetization including $S_i'^z$ and $m^z_{host} = \sum_{n\neq i} S_n^z$ is that of the host in the absence of impurity. m_{imp} should not be confused with the local magnetization of the impurity. We use $S = S' = 1$ hereafter. Defining the impurity susceptibility as $\chi_{imp} = \partial m_{imp}/\partial h$, Fig. 2 shows several regimes of screening of the impurity by the texture: partial, complete, and overscreening, as evidenced by $\chi_{imp} > 0$, ≈ 0, and < 0, respectively. This is consistent with a field-dependent fractional effective impurity spin [22], and is in a stark contrast with the collinear HAFs, where classical $m_{imp} \equiv S'$. The impurity magnetization is critical at h_s, as the susceptibility of the host is singular, similar to Ref. [25]. Fig. 2 also shows that the saturation in the system with impurity occurs above h_s of the pure host and that finite-size effects are negligible for the clusters and field ranges that we use.

For completeness, we note that the impurity-induced classical texture behaves singularly at $h \to 0$, although in a field range of measure zero in the thermodynamic limit — an effect also noted in [20, 28]. In a finite system, the energy gain of the canted state in Fig. 1, $\Delta E \sim -N^2h^2/(8S)$, is less than that of the state in which the Néel order of the host and the impurity spin both fully align with the field, $\Delta E = -hS'$. Thus, at $h = 0^+$ host spins are aligned (anti-aligned) with the field, $S_l^z = \pm S$. A spin-flop crossover to the textured state oc-

curs at $h_c \sim 8SS'/N^2 \to 0$ as $N \to \infty$. Inset (a) of Fig. 2 displays this behavior on *judiciously small* systems by monitoring the magnetization m_l^z of a spin at the largest geometrical distance from the impurity.

T-matrix.—We now turn to the spectral properties of the system. Because the texture breaks translational invariance, the Bogolyubov transformation of $\mathcal{H}_2$ has to be performed numerically [29]. The *para-unitary*, $2(N^2+1)\times 2(N^2+1)$ matrix $\mathbf{U}$ of this transformation maps the local Holstein-Primakoff bosons $\mathbf{a}^\dagger = [a_1^\dagger, \ldots, a_{N^2}^\dagger, a_i^\dagger, a_1, \ldots, a_{N^2}, a_i]$ onto Bogolyubov bosons $\bar{\mathbf{b}}^\dagger = [\bar{b}_1^\dagger, \ldots, \bar{b}_{N^2+1}^\dagger, \bar{b}_1, \ldots, \bar{b}_{N^2+1}]$, whose Hamiltonian, $\mathcal{H} = \bar{\mathbf{b}}^\dagger \mathbf{E} \bar{\mathbf{b}}/2$, is diagonal. The eigenenergies E_n are all positive except for $E_j = 0$ of the Goldstone mode. The Green's function in the $\bar{\mathbf{b}}$-basis is also a diagonal $2(N^2+1)\times 2(N^2+1)$ matrix $\mathbf{G}^{\bar{\mathbf{b}}}(z) = [z\mathbf{P} - \mathbf{E}]^{-1}$, where $\mathbf{P}$ is the para-unit matrix with $1(-1)$ in the upper (lower) half of its diagonal. The Green's function of the local Holstein-Primakoff bosons is $\mathbf{G}^{\mathbf{a}}(z) = (\mathbf{U}^\dagger)^{-1}\mathbf{G}^{\bar{\mathbf{b}}}(z)\mathbf{U}^{-1}$.

However, to formulate the scattering problem for the impurity-induced texture, the proper basis is that of the Bogolyubov magnons of the *uniform* host, which describe the incident and scattered magnons as plane-wave eigenstates of momentum $\mathbf{k}$. Thus, we first Fourier transform the matrix elements of $\mathbf{G}^{\mathbf{a}}(z)$ of the local *host* bosons to $\mathbf{k}$-space, yielding a matrix $\mathbf{G}^{\mathbf{a}}_{\mathbf{k}'\mathbf{k}}(z)$. Second, the host boson terms of this matrix are mapped onto the basis of the Bogolyubov magnons $\mathbf{b}^\dagger = [b_{\mathbf{k}}^\dagger, b_{\mathbf{k}}]$ of the *uniform* host, using the known parameters of the transformation, $u_{\mathbf{k}}$ and $v_{\mathbf{k}}$, for the square-lattice HAF in a field [26, 27]. This yields a matrix Green's function with three 2×2 substructures made from blocks of rank $N^2 \times N^2$, 1, and N. They correspond to the *dressed* (i) host magnon, (ii) impurity, (iii) and magnon-impurity Green's functions $\mathbf{G}_{\mathbf{k}'\mathbf{k}}(z)$, $\mathbf{G}_i(z)$, and $\mathbf{G}_{\mathbf{k}i}(z)$, respectively.

Altogether, starting from the numerical solution of the classical texture, followed by the real-space diagonalization of the harmonic problem and Bogolyubov transformation onto the uniform host, we obtain the dressed magnon Green's function $\mathbf{G}_{\mathbf{k}'\mathbf{k}}(z)$. From this we extract the scattering matrix $\mathbf{T}_{\mathbf{k}'\mathbf{k}}(z)$, focusing on the diagonal elements $\mathbf{T}_{\mathbf{k}\mathbf{k}}(z)$, which suffice to state our main findings:

$$\mathbf{T}_{\mathbf{k}\mathbf{k}}(z) = [\mathbf{G}^0_{\mathbf{k}}(z)]^{-2}\mathbf{G}_{\mathbf{k}\mathbf{k}}(z) - [\mathbf{G}^0_{\mathbf{k}}(z)]^{-1}\,, \qquad (2)$$

where $\mathbf{G}^0_{\mathbf{k}}(z)$ is the diagonal 2×2 Green's function of the uniform host magnons with $G^{0,11}_{\mathbf{k}}(z) = G^{0,22}_{\mathbf{k}}(-z) = [z - \varepsilon_{\mathbf{k}}]^{-1}$ and $\varepsilon_{\mathbf{k}}$ is the magnon energy.

No texture test.—First, we demonstrate the feasibility of obtaining the T-matrix from Eq. (2) numerically. For that purpose, we solve a complementary *artificial* problem, in which we neglect the feedback of the impurity on the host spins, i.e., spins in the plane retain their homogeneous field-induced canting of Fig. 1(b) and no texture is created. While such a reference state is unstable as $\mathcal{H}_{\rm class}$ is not at its minimum, it permits an analytical solution of the scattering problem of $\mathcal{H}_2$, details of which are provided in [27]. This solution generalizes the result of Ref. [30] to the case of finite fields with the goal of comparing it with the numerical procedure described above. In the following we consider the resolvent, i.e., the T-matrix stripped from the matrices of the Bogolyubov basis transformation $\mathbf{t}_{\mathbf{k}'\mathbf{k}}(z) = (\mathbf{B}^\dagger_{\mathbf{k}'})^{-1}\mathbf{T}_{\mathbf{k}'\mathbf{k}}(z)(\mathbf{B}_{\mathbf{k}})^{-1}$, where $B^{11(22)}_{\mathbf{k}} = u_{\mathbf{k}}$ and $B^{12(21)}_{\mathbf{k}} = v_{\mathbf{k}}$ [27].

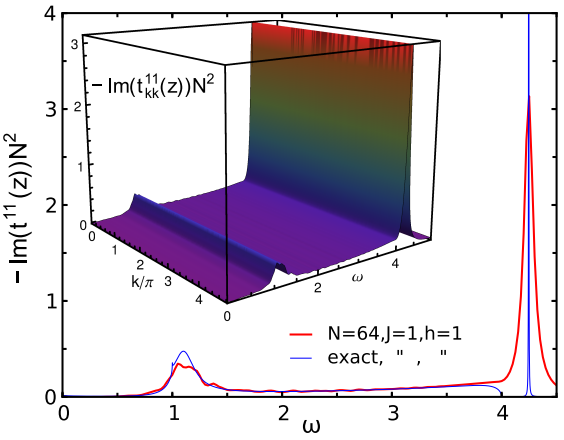

FIG. 3. (color online) Analytical and numerical results for the T-matrix spectrum in no-texture case, $J=1$, $h=1$. Homogeneous canting angles of the host spins $\theta \simeq 0.1253$. Impurity canting angle $\theta_i \simeq 0.8729$ as in the actual texture. Thin solid blue: exact $-\mathrm{Im}\, t^{11}(z{=}\omega)$ [27] with impurity resonance, $\omega{\approx}1.1$, and anti-bound state, $\omega{\approx}4.2$. Thick red solid: numerical $-\mathrm{Im}\, t^{11}_{\mathbf{k}'=\mathbf{k}=0}(z{=}\omega{+}i0.05)$ for $N{=}64$. Inset: numerical $-\mathrm{Im}\, t^{11}_{\mathbf{k},\mathbf{k}}(z{=}\omega{+}i0.05)$ along the $\mathbf{k}$-path of Fig. 4.

The analytical result for the the resolvent spectrum, $-\mathrm{Im}\, t^{11}_{\mathbf{k}'\mathbf{k}}(z)$, is plotted in Fig. 3 vs frequency ω. Naturally, $\mathbf{t}_{\mathbf{k}'\mathbf{k}}(z) \equiv \mathbf{t}(z)$ is *momentum independent* [27]. This is an expected behavior for scattering from point-like defects and is similar to scattering from vacancies in collinear HAFs [12, 13], where the resolvent shows some broad $\mathbf{k}$-modulation from superposition of a small number of partial waves. The inset of Fig. 3 shows $-\mathrm{Im}\, t^{11}_{\mathbf{k}\mathbf{k}}(z)$ obtained numerically from (2) along the path in $\mathbf{k}$-space shown in Fig. 4. Clearly, it is also momentum independent. In addition, analytical and numerical results, if evaluated on the finite clusters of the same size, agree to within numerical precision [27].

Finally, Fig. 3 demonstrates the spectral resolution we can obtain from the numerical procedure in an $N = 64$ cluster with a minimally acceptable imaginary broadening. One can see, that the numerical scattering amplitude has all the features of the analytical one: the impurity resonance, the shallow spin-wave continuum, and the anti-bound state above the upper edge of the spectrum [30]. Fine details, such as the anti-bound state gap and the non-analytic van Hove singularities are smeared out. Improving this with systems sizes beyond $N = 70$ is impractical because of the large memory requirements

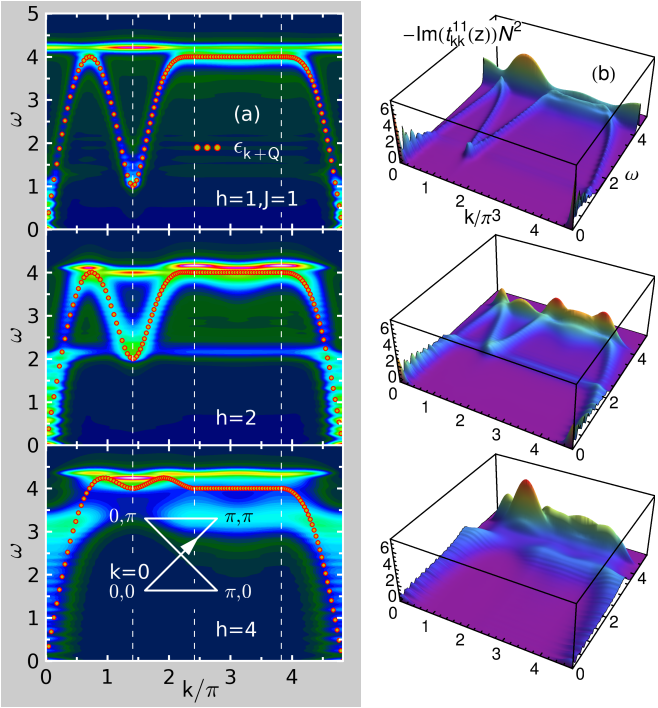

FIG. 4. (color online) The T-matrix resolvent spectra $-\mathrm{Im}\, t^{11}_{\mathbf{k},\mathbf{k}}(z{=}\omega{+}i0.05)$ in $N = 64$ cluster vs $\mathbf{k}$ and ω, $J = 1$, h=1, 2, and 4 along the depicted $\mathbf{k}$-path. Panel (a): contour plots superimposed with the shifted magnon dispersion $\varepsilon_{\mathbf{k}+\mathbf{Q}}$ (red-yellow dots). Dashed vertical lines: high-symmetry points along the $\mathbf{k}$-path. Panel (b): 3D plots.

for the non-sparse $2(N^2{+}1){\times}2(N^2{+}1)$ matrices.

Dispersive resonance.—We now consider the T-matrix for the true ground state of the system with spin texture. An analytical solution is not possible in this case. With the feasibility of the numerical procedure established, we evaluate the T-matrix from Eq. (2) using $\theta_{\{l\}}$ from the minimization of $\mathcal{H}_{\rm class}$ as an input to the Bogolyubov transformation. Representative results are shown in Fig. 4. Removing the $\mathbf{k}$-dependence due to transformation of the basis from $\mathbf{T}_{\mathbf{kk}}(z)$, we show $-\mathrm{Im}\, t^{11}_{\mathbf{kk}}(z)$ as a function of ω and $\mathbf{k}$ along a high-symmetry path in the Brillouin zone and for several values of the magnetic field. In Fig. 4, the radii of the textures are much smaller than the system size [27].

In a sharp contrast to the no-texture case, $\mathrm{Im}\, t^{11}_{\mathbf{kk}}(z)$ reveals a clear dispersive feature. The localized impurity resonance in Fig. 3 is now visible only as a faint maximum and is completely overshadowed by the dispersive resonance. Such a result is completely unexpected for the point-like impurity coupled to the Heisenberg model (1). Direct comparison in Fig. 4(a) shows that the $\mathbf{k}$-dependence of the dispersive resonance closely follows the spinwave dispersion $\varepsilon_{\mathbf{k}+\mathbf{Q}}$, folded by the ordering vector $\mathbf{Q} = (\pi, \pi)$. As one can see, the resonance is most sharply defined for small fields and gets washed out at higher fields. We find the dispersive feature to be prominent regardless of the system size or the impurity coupling J.

It is reasonable to suggest that the dispersive resonance is a natural outcome of the scattering from an extended region of the impurity-induced texture, arising due to non-collinearity of the state. This can be understood qualitatively from Fig. 1(c), which shows that the impurity spin has a component that acts as a local field in the direction perpendicular to the homogeneous field-induced canting. Because of that, the spins of Fig. 1(b) are perturbed from their local reference frames by the *staggered* transverse effective field. Then the spin-wave part of the Hamiltonian can be written as $\mathcal{H}_2 = \mathcal{H}^{h,i} + \mathcal{H}^{stag}$, where $\mathcal{H}^{h,i}$ contains the homogeneous canting of spins and the point-like impurity scattering as in the no-texture case, while $\mathcal{H}^{stag}$ is inhomogeneous with *staggered* matrix elements, which decay on the length scale set by the texture.

Because of the staggering, magnons must experience an umklapp scattering potential that can be approximated, for an extended region of the texture, as $\mathcal{H}^{stag} \sim \sum_{\mathbf{k}} \mathbf{W}_{\mathbf{k}} b^{\dagger}_{\mathbf{k}+\mathbf{Q}} b_{\mathbf{k}}$. Here, a qualitative analogy can be drawn with the 1D Kronig-Penney model whose T-matrix is dispersive and has a pole close to the zone-folded band ε_{k+Q} [31]. Because of the finite spatial extent of the texture, the dispersive resonance must be broadened. This is consistent with the increase of broadening in Fig. 4 at higher fields where the size of the texture shrinks. This may imply a nontrivial behavior of the T-matrix in the limit of $h \to 0$ where the texture becomes quasi-long-ranged [22]. We note that the impurity scattering does not lead to overdamping of the Goldstone mode, i.e., the spectral density at low energies in Fig. 4 does not occur at the ordering vector $\mathbf{Q}$.

Our results are of a direct relevance to the excitation spectra of non-collinear magnets with a low concentration x of impurities. Since the magnon self-energy is simply proportional to the diagonal element of the T-matrix via $\mathbf{\Sigma}_{\mathbf{k}}(\omega) \sim x\mathbf{T}_{\mathbf{kk}}(\omega)$, one may expect to observe an anomalous $\mathbf{k}$-dependent broadening of the spectrum where $\varepsilon_{\mathbf{k}}$ overlap with $\varepsilon_{\mathbf{k}+\mathbf{Q}}$ and an equally unusual field-dependence of such a broadening. Since the dynamical structure factor is directly related to the Green's function, these and other features should be observable by inelastic neutron scattering and specific predictions will be subject of future work.

Conclusions.—To conclude, we have presented strong evidence for a highly anomalous static and dynamic response of non-collinear antiferromagnets to doping by point-like defects. The scattering amplitude exhibits features that are strikingly different from usual s-wave scattering and include a highly dispersive resonance due to an impurity-induced texture. This result should be valid for the broad class of non-collinear magnets. Further theoretical and experimental studies seem highly desirable.

Part of this work has been done at the Kavli Institute for Theoretical Physics (A.L.C. and W.B.) and at the

Platform for Superconductivity and Magnetism, Dresden (W.B.). The work of A.L.C. was supported by the DOE under Grant No. DE-FG02-04ER46174. The work of W.B. was supported by DFG FOR912 Grant No. BR 1084/6-2, EU MC-ITN LOTHERM Grant No. PITN-GA-2009-238475, and the NTH SCNS. The research at KITP was supported by NSF Grant No. NSF PHY11-25915.

* w.brenig@tu-bs.de

[1] P. W. Anderson, Phys. Rev. **109**, 1492 (1958).
[2] A. A. Abrikosov and L. P. Gorkov, Sov. Phys. JETP **12**, 1243 (1961) [ZhETF **39(6)**, 1781 (1960)].
[3] P. W. Anderson, Phys. Rev. Lett. **18**, 1049 (1967).
[4] O. P. Vajk, P. K. Mang, M. Greven, P. M. Gehring, and J. W. Lynn, Science **295**, 1691 (2002).
[5] A. W. Sandvik, Phys. Rev. Lett. **89**, 177201 (2002).
[6] T. Vojta and J. Schmalian, Phys. Rev. Lett. **95**, 237206 (2005).
[7] R. Yu, T. Roscilde, and S. Haas, Phys. Rev. Lett. **94**, 197204 (2005).
[8] A. W. Sandvik, Phys. Rev. Lett. **96**, 207201 (2006).
[9] G. B. Martins, M. Laukamp, J. Riera, and E. Dagotto, Phys. Rev. Lett. **78**, 3563 (1997).
[10] S. Sachdev, C. Buragohain, and M. Vojta, Science **286**, 2479 (1999).
[11] K. H. Höglund and A. W. Sandvik, Phys. Rev. Lett. **91**, 077204 (2003).
[12] W. Brenig and A. P. Kampf, Phys. Rev. B **43**,12914 (1991).
[13] A. L. Chernyshev, Y. C. Chen, and A. H. Castro Neto, Phys. Rev. Lett. **87**, 067209 (2001); Phys. Rev. B **65**, 104407 (2002).
[14] S. Dommange, M. Mambrini, B. Normand, and F. Mila, Phys. Rev. B **68**, 224416 (2003).
[15] G. B. Martins and W. Brenig, J. Phys.: Cond. Matt. **20**, 415204 (2008).
[16] C. Weber and F. Mila, preprint, arXiv:1207.0095.
[17] R. R. P. Singh, Phys. Rev. Lett. **104**, 177203 (2010).
[18] D. Poilblanc and A. Ralko, Phys. Rev. B **82**, 174424 (2010).
[19] A. J. Willans, J. T. Chalker, and R. Moessner, Phys. Rev. B **84**, 115146 (2011).
[20] A. Wollny, E. C. Andrade, and M. Vojta, Phys. Rev. Lett. **109**, 177203 (2012).
[21] S. Eggert, O. F. Syljuåsen, F. Anfuso, and M. Andres, Phys. Rev. Lett. **99**, 097204 (2007).
[22] A. Wollny, L. Fritz, and M. Vojta, Phys. Rev. Lett. **107**, 137204 (2011).
[23] C. Henley, Can. J. Phys. **79**, 1307 (2001).
[24] A. Lüscher and O. P. Sushkov, Phys. Rev. B **71**, 064414 (2005).
[25] M. E. Zhitomirsky and T. Nikuni, Phys. Rev. B **57**, 5013 (1998).
[26] M. Mourigal, M. E. Zhitomirsky, and A. L. Chernyshev, Phys. Rev. B **82**, 144402 (2010).
[27] See Supplemental Material at http://link.aps.org/-supplemental for details of the calculations of the static and dynamical properties of the model (1).
[28] After completion of our work, we became aware of the study [20], reporting similar findings but for different types of host spin systems and impurities.
[29] J. H. P. Colpa, Physica A **93**, 327 (1978).
[30] J. Igarashi, K. Murayama, and P. Fulde, Phys. Rev. B **52**, 15966 (1995).
[31] M. P. Marder, *Condensed Matter Physics*, (Wiley, New Jersey, 2010).